Available online at www.sciencedirect.com
SCIENCE DIRECT®
Journal of Nuclear Materials 324 (2004) 189–197
journal of nuclear materials
www.elsevier.com/locate/jnucmat

Bulk and Young's modulus of doped UO_2 by synchrotron diffraction under high pressure and Knoop indentation

M.C. Pujol [a], M. Idiri [a], L. Havela [a,b], S. Heathman [a], J. Spino [a,*]

[a] European Commission, Joint Research Centre, Institute for Transuranium Elements, P.O. Box 2340, D-76125 Karlsruhe, Germany
[b] Charles University, Ke Karlovu 5, 121 16 Prague 2, Czech Republic

Received 31 July 2003; accepted 4 October 2003

Abstract

The elastic constants of doped UO_2 simulating a burn-up in the reactor of up to 200 GWd/t M (≃20% U-atoms replaced by fission products) were measured by synchrotron diffraction under high pressure and by Knoop indentation. As a complement, also the corresponding thermal expansion was determined by X-ray diffraction at high temperature. It is shown that the elastic constants of the simulated fuels are increased with burn-up, while the thermal expansion is decreased, satisfying the Grüneisen equation. An increasing Grüneisen constant γ with burn-up is also suggested. The results are, however, in contradiction with empirical bulk modulus estimates and previous data from ultrasonic measurements indicating either slightly decreasing or unchanged to strongly decreasing stiffness with burn-up. The need to perform detailed cohesive energy calculations of the doped fuel (ab initio or empirical potential methods), as well as to review the role of microstructure heterogeneities in the ultrasonic *E*-modulus determinations are therefore suggested.

1. Introduction

The elastic properties of UO_2 have been matter of study over many decades, since the compound is used as fuel material in nuclear reactors [1–6]. Their application refers particularly to reactor-transient and pellet-cladding-mechanical-interaction (PCMI) situations under which creep is unlikely [1]. Under these situations the Young's modulus (E), together with the thermal expansion and thermal conductivity, determines principally the level of the tangential or hoop stress in the fuel during a power ramp, and the resulting crack-pattern [7,8]. On the other hand, as it depends on the interatomic forces, the elastic modulus is indicative of the evolution of the bond strength of the fuel in the course of irradiation.

Initially, the elastic modulus of UO_2 was studied as a function of the porosity [1–5], the oxygen-to-metal ratio (O/M) [6], the grain size [5], the dopant concentration [3] and temperature [1–3], using predominantly ultrasonic techniques. As for the room temperature measurements, the results indicated a monotonic decrease of the Young's modulus with the porosity and the O/M ratio [1–6], though almost no variation with the grain size [5] and the dopant concentration [3]. The latter studies covered simulated fuels with up to 6% burn-up and 1% Gd_2O_3-doped UO_2 [3]. Other studies with single-oxide doping indicated an increase of the *E*-modulus with silica, zirconia and ceria additions, but a decrease with beryllia addition [3,9]. Furthermore, measurements with (U, Pu) oxides revealed a moderate increase of the elastic modulus from 4% to 11% in comparison to pure UO_2, for Pu-concentrations between 15% [10,11] and 70% [10,12]. However, additions of 6 wt% fission products to a $U_{0.8}Pu_{0.2}O_2$ fuel produced a small decrease of the elastic modulus with respect to the undoped mixed-oxide fuel [4,10].

More recent studies applying a local micro-acoustic technique showed consistency with previous results concerning the variation with porosity [13,14] and grain

* Corresponding author. Tel.: +49-7247 951 233; fax: +49-7247 951 590.
E-mail address: jose.spino@itu.fzk.de (J. Spino).

0022-3115/$ - see front matter © 2003 Elsevier B.V. All rights reserved.
doi:10.1016/j.jnucmat.2003.10.002

size [15]. However, discrepancies appeared with regard to the variation with the dopant concentration, since significantly decreased E-moduli were measured for simulated UO_2 fuels with burn-ups up to 80 GWd/t M [16] (≈8 at.% burn-up). Also, relatively recent ultrasonic pulse-echo measurements in Ce-doped UO_2 showed about 30% decrease of the E-modulus for 20 mol% addition of CeO_2 [17], with even further decrease on additional Zr and Nd doping [18].

In view of these somewhat contradictory results regarding the influence of the fission products and the lack of data at high burn-up, it was our intention to determine the elastic modulus of doped UO_2 fuels by other methods than the ultrasonic technique. For this purpose, the technique of synchrotron powder diffraction at high pressures [19] was selected, to determine the lattice compressibility (or bulk modulus) of the solid with essentially no contribution of the microstructure and secondary-phase inclusions. In parallel, confirmation was sought by the Knoop indentation technique, which provides the Young's modulus-to-hardness ratio (E/H) of materials with an error <10% [20], and from which the E-value can be obtained by separately measuring the hardness by Vickers indentation.

2. Experimental procedure

2.1. Synchrotron powder diffraction at high pressures

The method is routinely applied at the ITU Karlsruhe to characterise the high-pressure behaviour (e.g. bulk modulus and phase transitions) of actinide and lanthanide compounds, and has been described elsewhere [19,21]. The technique consists of measuring the change of the lattice constants as a function of the applied pressure. The zero-pressure bulk modulus (B_0) is accurately determined by fitting the results with the Birch [22] and Murnaghan [23] equations of state, from which also the pressure derivative of the bulk modulus (B_0') is obtained.

In the present case the synchrotron radiation source at the facility Hasylab, DESY, Hamburg, Germany, was used, with an incident beam cross-section of about 50×50 μm. A configuration of energy dispersive detector and fixed Bragg angle ($\theta \cong 5.45°$) was used. The valid diffraction equation is $2d(hkl)\sin\theta = ch/E$, where $d(hkl)$ = interplanar spacing, θ = Bragg angle, c = velocity of light, h = Planck's constant and E = photon energy. The experimental errors in the Bragg angle and energy determinations were, respectively, ±0.03° and ±0.05 keV. The sample was compressed by means of a diamond anvil cell of the Syassen–Holzapfel type. For the experiments only a small amount of (crushed) sintered sample was used, which was loaded into a 200 μm-hole drilled into an Inconel gasket, which was filled with the pressure-transmitting media (silicon oil). Together with the sample also a ruby chip was loaded, whose known fluorescent wavelength shift with pressure under laser excitation was used to calibrate the applied pressure [19,21]. The accuracy in this pressure determination was about ±0.5 GPa.

Since the silicon oil used solidifies roughly above 10 GPa, causing errors in the volume–pressure determinations due to broadening of the sample and ruby fluorescence lines [21], only the experimental data below this pressure limit were considered. Crushing of the samples was assumed to eliminate the fabrication porosity. The results were thus considered to correspond to the 100% dense material.

2.2. Knoop indentation tests

The utilisation of indentation tests to evaluate the E-modulus of materials is based on the demonstration [24] that the extent of the elastic recovery (of the residual depth) after indentation is related to the H/E ratio of the material, where H is the corresponding hardness. For a strongly asymmetric Knoop-pyramid indenter, where the long diagonal (a) is 7.11 times larger than the short one (b), the relationship $b'/a' = b/a - \alpha H/E$ has been verified, where b'/a' is the ratio of the remaining imprint diagonals and α is a constant [20]. Thus, with a calibration curve for a wide range of well characterised materials, the H/E ratio of a given material can be estimated via its measured b'/a' ratio, with an error <10% principally for brittle materials [20].

For the present experiments, an enlarged calibration curve 'b'/a' vs. H/E' was obtained. This included the original data of [20] and five additional reference materials that extended the H/E range. For these materials the E-values were determined by instrumented indentation, in three cases by a certification Institute [25] and in two cases in our laboratories. The corresponding H values were determined by averaging the results of at least ten Vickers indentations at 10 N (same load as in [20]). The b'/a' values were assigned by averaging the results of at least five Knoop indentations at the loads 5, 10 and 20 N, performed on metallographic samples. The evaluation of the imprint dimensions was done by optical microscopy. The average b'/a' ratios of the fuel materials were determined by the same procedure, though only at the indentation load 10 N. Their corresponding E values were deduced by extracting E/H from the extended calibration curve, and by taking into account the H values determined in a previous work [26].

2.3. Samples

The specimens studied were a sintered UO_2 pellet with >95% theoretical density, and simulated fuels of

various origins, covering the burn-up range 0–200 GWd/t M. The simulated fuels included three commercial samples provided by AECL (Atomic Energy of Canada Limited) with the trademark SIMFUEL [27], with burn-ups 3, 6 and 8 at.%, and own samples in the range 35–200 GWd/t M prepared by both dry and wet-chemistry routes. Similar to the commercial samples [27], the preparation of our simulated fuels by the dry method required co-mixing of UO_2 and (simulated) fission products oxide powders, followed by pre-calcination at 950 °C, re-milling, cold-pressing and sintering at 1640 °C [28]. The characterisation of these samples is described in [28]. Their nominal cation composition, according to [28], is shown in Table 1.

Whereas in the samples prepared by the dry method a homogeneous distribution of U and fission products atoms is achieved only after high-temperature treatment, in the simulated fuel prepared by the wet-chemistry route, the same is achieved in the early steps of the process. In the applied liquid-mix (or Pechini) method [29], adequate quantities of uranium dioxide and (simulated) fission products nitrates are dissolved in nitric acid to form a mixed nitrate by evaporation, which is then re-dissolved and polymerised by respective additions of citric acid and ethylene glycol. The result is a precursor chelate compound (polymeric resin), in which all cations are mixed at atomic level. The formation of the mixed oxide is verified after calcination in air at 600–800 °C [29]. This is completed during final sintering (under $Ar + H_2$ gas, at 1640 °C), after conditioning and cold pressing. A thorough description of the method will be given in [30].

Care was taken to keep the O/M ratio of all samples in the range 2.000 ± 0.001 by the procedure described in [28]. As the exact composition analysis of the liquid-mix sample is not yet available, its nominal burn-up was used in this work.

3. Results

3.1. Bulk modulus (B_0) of doped UO_2 from synchrotron compressibility tests

For the bulk modulus determinations via compressibility tests, the AECL–SIMFUEL 3 and 8 at.% samples were used, as well as the 20 at.% sample prepared in our laboratories by the liquid-mix method. For comparison, data corresponding to a standard UO_2-sample examined previously at the synchrotron of ESFR-ILL, Grenoble, France, in a diamond anvil cell (Syassen–Holzapfel type) [31] are also included.

Fig. 1 shows the high-(*hkl*) part of the diffraction diagrams of the doped fuels at comparable pressures, indicating clearly a progressive shift of the Bragg peaks towards lower photon energies as burn-up increases. For

Table 1
Nominal cation composition of some ITU-simulated UO_2 spent fuels [28]

Element	Wt% metal				
	Burn-up (GWd/t M)				
	25	70	115	150	200
Ce[a] (Ce, Np, Pu)	0.71	1.33	1.70	1.96	2.31
La (La, Am, Cm)	0.09	0.32	0.61	0.81	1.15
Rb	0.03	0.06	0.09	0.11	0.14
Sr	0.07	0.15	0.21	0.26	0.33
Zr	0.34	0.70	1.03	1.31	1.71
Mo	0.29	0.71	1.13	1.47	1.97
Ru (Tc)	0.26	0.69	1.22	1.59	2.07
Rh	0.04	0.07	0.08	0.08	0.09
Pd	0.06	0.42	0.86	1.19	1.75
Ag	0.01	0.02	0.03	0.03	0.04
Cd	0.00	0.04	0.11	0.17	0.29
Te	0.04	0.10	0.17	0.22	0.30
Cs	0.24	0.53	0.82	1.04	1.37
Ba	0.12	0.35	0.57	0.78	1.08
Pr	0.11	0.23	0.34	0.44	0.56
Pm (Nd)	0.32	0.85	1.35	1.76	2.74
Sm	0.06	0.15	0.21	0.24	0.27
Gd (Eu)	0.01	0.10	0.24	0.36	0.65
U	97.16	93.10	89.12	86.04	81.01

[a] Head element of the line replaced all following elements within parenthesis according to the sum of the respective atomic concentrations in the real fuel.

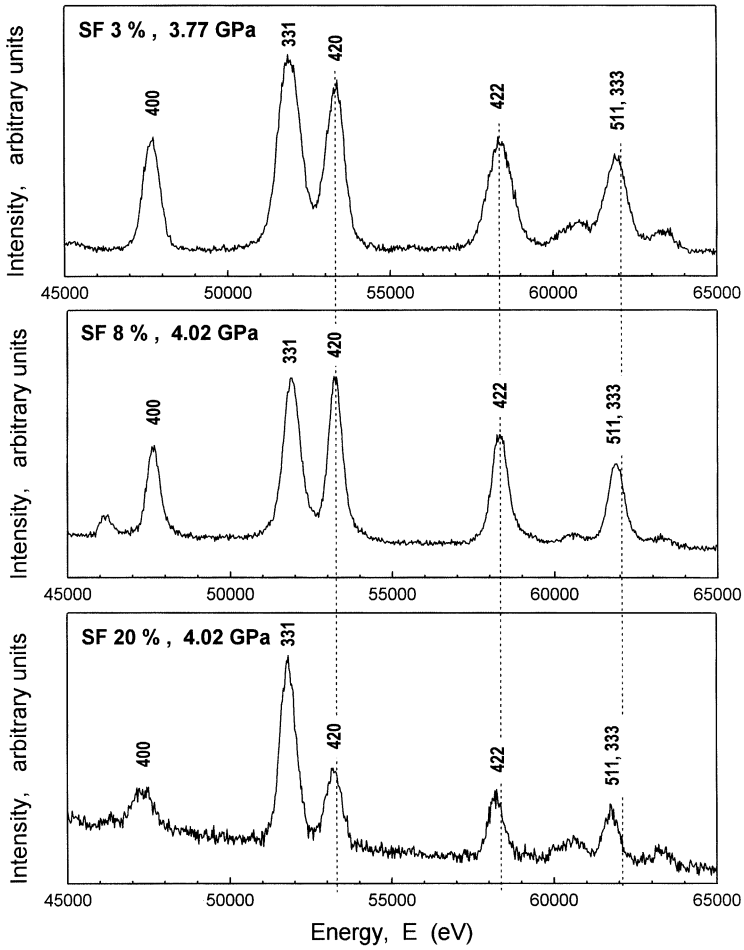

Fig. 1. Partial diffraction diagrams of the simulated fuels at equivalent pressures showing progressive displacement of the peaks towards lower energies on increasing burn-up.

a constant diffraction angle, the results indicate a smaller lattice parameter decrease at similar pressures, and therefore less compressibility of the fuel, with increasing burn-up. This can be also visualised in Fig. 2 where the relative unit cell volume $V/V_0 = (a/a_0)^3$, with a_0 and a being the fuel lattice constants at ambient and high pressures, are plotted vs. the applied pressure (p). The decreasing compressibility (or increasing B_0 modulus) is evidenced by the decreasing slope of the curves at increasing burn-ups.

The determination of the B_0 and B_0' values was done by curve fitting with the appropriate equations of state. Apart from the usual Birch [22] and Murnaghan [23] equations mentioned in Section 2.1, also other functions proposed by Holzapfel [32], Vinet et al. [33] and Kumar [34] were considered. These equations as well as the B_0 and B_0' values, their error bands (n) and the correlation (or fitting quality) factors (r^2) are quoted in Table 2. As can be seen, in the low-pressure range of this study, there is essentially no difference in the results among the different equations used. The resulting B_0 values clearly indicate an increasing stiffness of the UO_2 lattice as burn-up increases.

For the case of UO_2, the B_0 value is found compatible with the elastic modulus (E) determined by other techniques. By application of the expression $E = 3B_0(1–2\nu)$, with ν = Poisson's ratio and with $\nu(UO_2) = 0.319 \pm 0.004$ [10], the deduced E-modulus is $E(UO_2) = 216 \pm 6$ GPa. This value agrees well with the average value $E(UO_2) = 223 \pm 3$ GPa recommended in the review [10].

As for the simulated fuels, a Poisson ratio of $\nu(SF) = 0.31 \pm 0.04$ is assumed, which corresponds to the average of values quoted in [3] (fuels with $\leqslant 6$ at.% burn-up), after their correction to zero porosity. The deduced E-moduli show the same increasing trend with burn-up as the measured B_0-values, with up to 70% in-

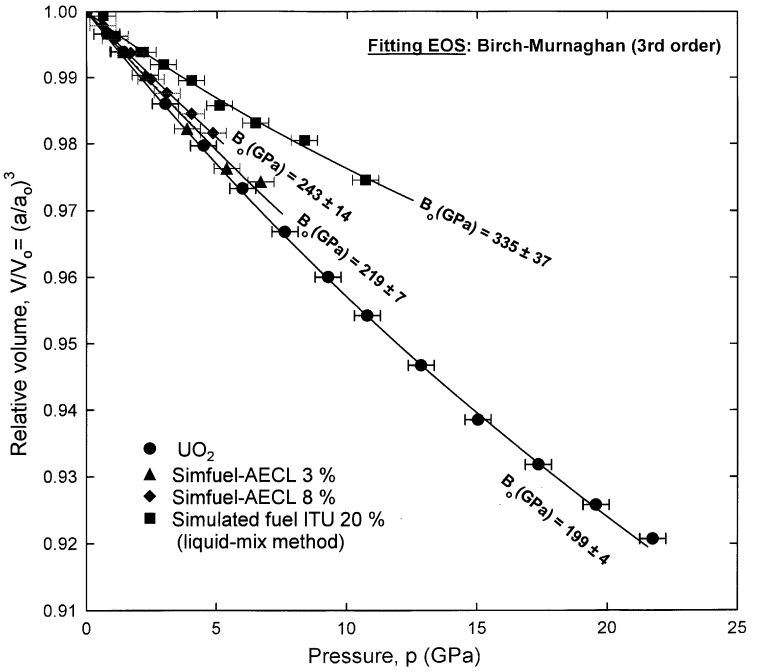

Fig. 2. Compressibility curves of UO_2 and simulated low and high burn-up fuels showing increasing bulk modulus (B_0) with burn-up according to Table 1.

Table 2
Calculated bulk moduli B_0 and their first pressure derivatives B'_0 according to various fitting equations of state (EOS)

EOS	UO_2 ($p \leqslant 22$ GPa)			SIMF 3% ($p \leqslant 6.7$ GPa)			SIMF 8% ($p < 5$ GPa)			SIMF 20% ($p \leqslant 10.7$ GPa)		
	B_0	B'_0	r^2	B_0	B'_0	r^2	B_0	B'_0	r^2	B_0	B'_0	r^2
(a)	199(4)	6.1(0.6)	0.999	219(7)	6.5 (*)	0.987	243(14)	6.5(7)	0.997	336(36)	17(10)	0.997
(b)	198(4)	6.5(0.6)	0.999	219(7)	6.5 (*)	0.987	244(13)	6.5(7)	0.997	332(22)	20(8)	0.994
(c)	198(4)	6.5(0.6)	0.999	219(7)	6.5 (*)	0.987	243(14)	6.5(7)	0.997	335(31)	18(9)	0.994
(d)	198(4)	6.6(0.6)	0.999	219(7)	6.5 (*)	0.987	243(14)	6.5(7)	0.997	334(31)	18(9)	0.994
(e)	198(4)	6.4(0.6)	0.999	219(7)	6.5 (*)	0.987	243(14)	6.5(7)	0.997	336(37)	17(10)	0.994

(a) Murnaghan [23], $p = B_0/B'_0((V/V_0)^{-B'_0} - 1)$. (b) Birch–Murnaghan [22], $p = 3/2B_0((V/V_0)^{-7/3} - (V/V_0)^{-5/3})(1 - 3/4(4 - B'_0)((V/V_0)^{-2/3} - 1))$. (c) Holzapfel [32], $p = 3B_0((V/V_0)^{-5/3} - (V/V_0)^{-4/3})\exp(3/2(B'_0 - 3)(1 - (V/V_0)^{1/3}))$. (d) Vinet et al. [33], $p = 3B_0((V/V_0)^{-2/3} - (V/V_0)^{-1/3})\exp(3/2(B'_0 - 1)(1 - (V/V_0)^{1/3}))$. (e) Kumar [34], $p = B_0/(B'_0 + 1)(\exp((B'_0 + 1)(1 - V/V_0)) - 1)$. r^2 = correlation (fraction of variance explained).
(n) = error band of fitted parameter, (*) = fixed parameter.

crease at 200 GWd/t M burn-up with respect to pure UO_2. However, this trend does not coincide, with the existing data in the literature, which show almost no dependence with burn-up [3,10] or decreasing E-values with burn-up [16–18].

3.2. Young's modulus (E) from Knoop indentation tests

The Knoop indentation tests provide a practical way to determine the E-modulus of materials from the measurement of the residual imprint diagonals ratio b'/a'. This is done by extracting the H/E ratio from a calibration curve b'/a' vs. H/E and by determining H separately. The calibration curve done for this work is shown in Fig. 3. Using the linear fitting $b'/a' = b/a - \alpha H/E$, the parameters obtained are $b/a = 0.143 \pm 0.001$ and $\alpha = 0.498 \pm 0.019$. It is noted that the correlation crosses the y-axis at 0.143, which is only slightly higher than the nominal value 0.141 for ideally plastic materials ($H/E \to 0$) [20].

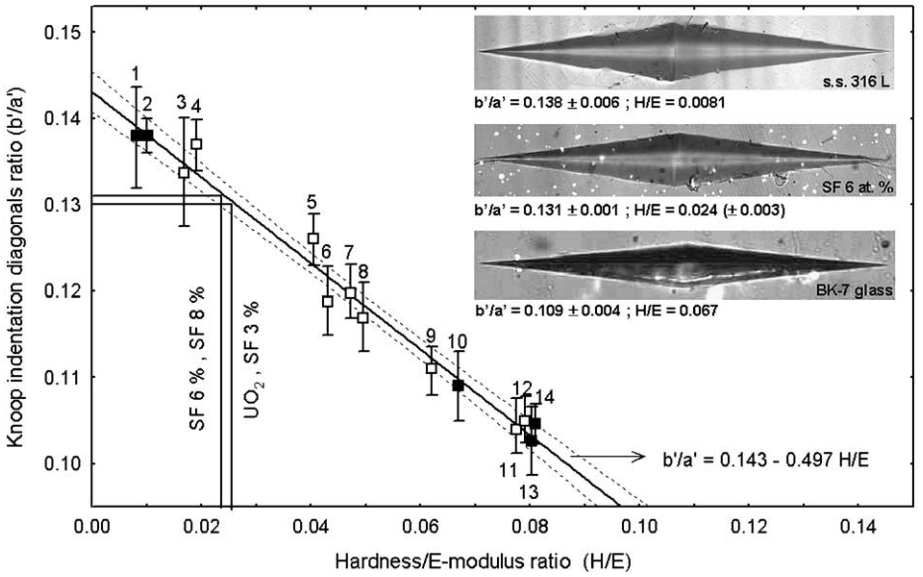

Fig. 3. Calibration curve b'/a' vs. H/E. Micrographs of indented 316 L stainless steel, SIMFUEL 6 at.% and BK-7 glass, showing increasing elastic recovery (flatter imprints) at correspondingly increasing H/E ratios. Reference materials – this work: (1) stainless steel 316 L, (2) W-alloy, (10) BK-7 glass, (13) nylon, (14) polyethylene. From [21]: (3) ZnO, (4) ZnS, (5) hardened steel, (6) MgF_2, (7) ZrO_2, (8) Al_2O_3, (9) Si_3N_4, (11) glass-ceramic, (12) soda-lime glass.

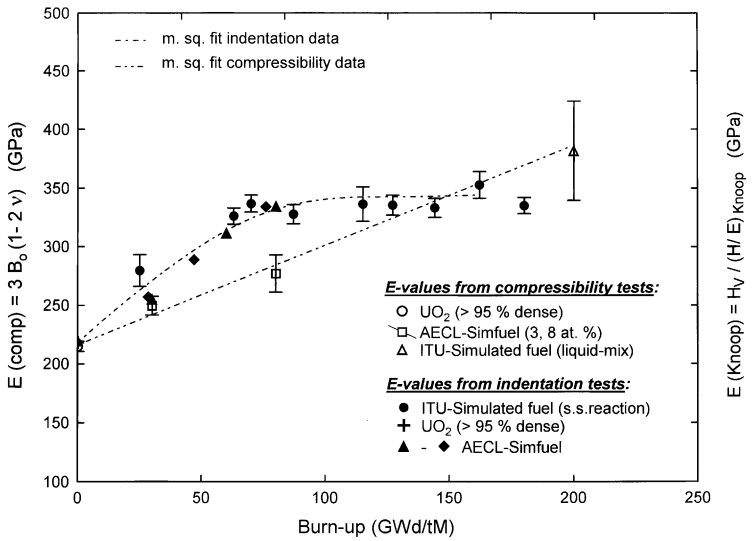

Fig. 4. Comparison of Young's modulus values arising from compressibility and indentation tests.

The measured b'/a' values of the samples UO_2 (>95% th.d.) and the AECL-simulated fuels (SF) with 3, 6 and 8 at.% burn-up are also given in Fig. 3. The deduced H/E ratio for the samples UO_2 and SF 3 at.% is 0.026. For the samples SF 6 and 8 at.% this is 0.024. The first value coincides with the value $H/E = 0.0263$ determined elsewhere for dense UO_2 [35]. According to the 95% confidence limits of the calibration curve of Fig. 3, the scatter band of the deduced H/E values is about 10%. The same is valid for the result of [35], which arises from the same experimental method.

The H values determined previously in [26] by Vickers indentation were converted to E values, assuming the H/E ratio to remain equal to 0.024 at burn-ups above 80 GWd/t M. The results are shown in Fig. 4 as a function of burn-up, and are also compared with the values deduced from the compressibility tests of Section 3.1. Good coincidence of the two kinds of measurements is obtained for pure UO_2. With increasing burn-up, increasing, though not fully overlapping trends were observed for the two kinds of values (Fig. 4). However, the agreement is considered satisfactory, as the converted values are very sensitive to the constants H/E and v. In Fig. 4 the scatter bands arising only from the B_0 and H determinations are shown. If scatters of the constants H/E and v are included, obviously much larger error bands would exist.

Finally, the saturation of the $E(H)$ values determined by indentation for burn-ups above 80 GWd/t M (Fig. 4) is noted. This may be due partially to the saturation of the fission-products dissolution in UO_2, particularly in the solid state reacted samples [28].

4. Discussion

The two somewhat different sort of experiments, i.e. the physical bulk modulus (B_0) determination through lattice compression (atomic scale) and the H/E determination via indentation (meso-microscopic scale) show coincident results. The elastic moduli (E) derived in both cases indicate that dissolution of fission products causes the fuel stiffness to substantially increase during irradiation, namely at a rate of $\simeq$3.5% per 10 GWd/t M of burn-up. For example, at the burn-up possibly reached in the rim zone of highly exposed LWR fuels ($\simeq$200 GWd/t M), an increase of about 70% of the original fuel stiffness is to be expected. Since, in addition to the chemical effects, the structural defects generated during irradiation would modify predominantly the plastic behaviour (dislocation motion) [7], the elastic behaviour observed here is assumed to approach that in the reactor, except for the influence of porosity.

From the point of view of the interatomic forces, the above results indicate increasing bond strength of the fuel with increasing burn-up. This would imply also a larger rigidity of the lattice against temperature variation, which implies a lower thermal expansion (Grüneisen relation, $\alpha B = \gamma C_v/V$, where $\alpha =$ thermal expansion, $B =$ isothermal bulk modulus, $C_v =$ heat capacity at constant volume, $V =$ molar volume and $\gamma =$ Grünensein constant [36,37]) and a higher Debye temperature $(\theta_D = (1/k_B)(6\pi^2/V)^{1/3}(B_s/M)^{1/2}$, where $\theta_D =$ Debye Temperature, $k_B =$ Boltzmann constant, $B_s =$ adiabatic bulk modulus and $M =$ compound molecular mass [38,39]).

To our knowledge there are no experimental data regarding the variation of θ_D with burn-up. However, recent neutron powder diffraction experiments on low burn-up simulated Dupic fuel (10–20 GWd/t M) [40] show, in contradiction with the above, a slightly increased thermal expansion compared to UO_2. To elucidate this discrepancy, high temperature XRD

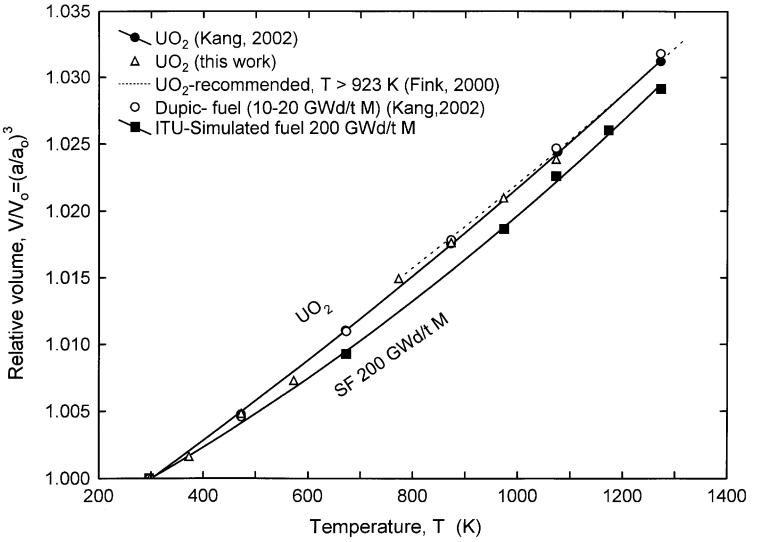

Fig. 5. High-temperature XRD thermal expansion curves for UO_2 [40,41], Dupic fuel (estimated 10–20 GWd/t M) [40] and the present simulated fuel with nominal 200 GWd/t M burn-up. Measurements under protective-reducing ($Ar–H_2$) atmosphere.

experiments have been undertaken with our materials, the preliminary results of which are shown in Fig. 5. Specific details of these measurements will be given elsewhere [41]. Fig. 5 shows also the data of Ref. [40] and the recommended thermal expansion curve for UO_2 at >923 K [42].

For our high burn-up sample (200 GWd/t M) a reduced thermal expansion relative to UO_2 was observed (Fig. 5). However, by virtue of the Grüneisen equation, the observed thermal expansion decrease ($\simeq$10%) appears not to compensate for the measured B_0 increase ($\simeq$70%) (Section 3.1), since the C_v/V ratio would change only little with burn-up. Certainly, the specific heat at constant pressure, C_p, was shown to increase very slightly with burn-up ($C_p(80\ \mathrm{GWd/t\,M}) \cong 1.008 C_p(UO_2)$ [43]). On the other hand, the lattice constant (a), and hence the molar volume ($V \cong a^3$), decreases only slightly with burn-up ($a(200\ \mathrm{GWd/t\,M}) \cong 0.998 a(UO_2)$ [28]). The above may imply an increase of the constant γ with burn-up, though this awaits confirmation. To verify the observed trends, independent measurements of θ_D appear worthwhile.

In spite of the above consistency of the B_0, E and α parameters, the measured increase of the elastic constants with burn-up does not agree with empirical estimates and some pre-existing experimental data.

A slight decrease of the bulk modulus of the fuel is predicted by the model of Hazen and Finger [44,45] with increasing burn-up. The model postulates for oxide compounds $B \simeq 750\ (z/d'^3)$ GPa, with z = cation formal valence and d' (0.1 nm) = cation oxygen bond distance (for fcc crystals $d' = 1/4(3a^2)^{1/2}$, a = lattice constant). Thus, whereas it correctly predicts $B \simeq 225$ GPa for pure UO_2 ($z = 4$, $a = 0.5457$ nm) [45], it predicts only $B \simeq 221$ GPa for the fuel with 200 GWd/t M burn-up. This is due to the reduced cation valence of fuel at this burn-up (>11% trivalent dissolved fission products (Table 1): $z \leqslant 3.9$), combined with the slightly decreased lattice constant ($a = 0.547$ nm at 200 GWd/t M burn-up [28]). However, since these are only preliminary estimates, more detailed atomic calculations, e.g. using ab initio [46,47] or empirical potentials [48,49] methods, will be needed.

Finally, the present results remain in conflict with earlier [3] and more recent work [16–18], which applied ultrasonic techniques. These studies showed either unchanged or moderately to strongly decreasing E-moduli of the UO_2 fuels (simulated or irradiated) up to burn-ups around 80 GWd/t M. However, it is important to note that the ultrasonic technique, usually involving large samples (up to several cm), is very sensitive to material heterogeneities (porosity, cracks, second phase precipitates, etc.). On the contrary, the two presently applied techniques (nm or μm range) give mainly information on the elasticity of the lattice. An influence of the microstructure to explain the above-mentioned discrepancies is therefore very likely.

5. Conclusions

Both compressibility and indentation results show that the elastic constants of UO_2 are increased in the course of irradiation as fission products replace the fissioned U-atoms in the lattice. The observed increased stiffness is also consistent with a decreased thermal expansion according to the Grüneisen relation. An increase in the Grüneisen constant γ with burn-up is also suggested.

The results, however, contradict empirical bulk modulus estimates and previous experimental results using the ultrasonic technique. These indicate either independent or decreasing E-moduli with burn-up. To elucidate these discrepancies, detailed cohesive energy calculations of the doped fuel employing ab initio or empirical potential methods, as well as further studies on the role of microstructure defects on ultrasonic E-modulus measurements, are recommended.

References

[1] A.R. Hall, AERE-R-5650, 1967. Also in, J. Nucl. Mater. 37 (1970) 314.
[2] R.J. Forlano, A.W. Allen, R.J. Beals, J. Am. Ceram. Soc. 50 (1967) 93.
[3] M.O. Marlowe, A.I. Kaznoff, in: Ceramic Nuclear Fuels, International Symposium, 3–8 May 1969, Washington, DC, The American Ceramic Society, Ohio, USA, 1969.
[4] J. Boocock, A.S. Furzer, J.R. Matthews, AERE-M 2565, 1972.
[5] N. Igata, K. Domoto, J. Nucl. Mater. 45 (1972/73) 317.
[6] R.J. Forlano, A.W. Allen, R.J. Beals, J. Am. Ceram. Soc. 51 (1967) 192.
[7] D.R. Olander, Fundamental Aspects of Nuclear Reactor Fuel Elements, TID-26711-P1, 1976.
[8] L.O. Jernkvist, Nucl. Eng. Des. 176 (1997) 273.
[9] D.J. Bowers, W.A. Hedden, J.M. Snyder, W.H. Duckworth, Battelle Memorial Institute Report, BMI-1177, 1956.
[10] D.G. Martin, High Temp. – High Press. 21 (1989) 13.
[11] C.H. de Novion, B. Amice, A. Groff, Y. Guerin, A. Padel, in: W.N. Miner (Ed.), Plutonium 1970 and Other Actinides, Nucl. Met. 17 (1970) 509.
[12] A.W. Nutt, A.W. Allen, J.H. Handwerk, J. Am. Ceram. Soc. 53 (1970) 205.
[13] V. Roque, D. Baron, J. Bourgoin, J.M. Saurel, J. Nucl. Mater. 275 (1999) 305.
[14] V. Roque, B. Cros, D. Baron, P. Dehaudt, J. Nucl. Mater. 277 (2000) 211.
[15] D. Laux, B. Cros, G. Despaux, D. Baron, J. Nucl. Mater. 300 (2002) 192.
[16] D. Laux, G. Despaux, D. Baron, J. Spino, in: 7th International Conference on CANDU Fuel, Kingston, Ont., Canada, 23–27 September 2001.
[17] K. Yamada, S. Yamanaka, T. Nakagawa, M. Uno, M. Katsura, J. Nucl. Mater. 247 (1997) 289.

[18] S. Yamanaka, S. Yoshida, K. Kurosaki, M. Uno, K. Yamamoto, T. Namekawa, J. Alloys Compd. 327 (2001) 281.
[19] S. Heathman, T. Le Bihan, S. Darracq, C. Abraham, D.J.A. De Ridder, U. Benedict, J. Mattenberger, O. Vogt, J. Alloys Compd. 230 (1995) 89.
[20] D.B. Marshall, T. Noma, A.G. Evans, J. Am. Ceram. Soc. 65 (1982) C175.
[21] Y. Méresse, S. Heathman, T. Le Bihan, J. Rebizant, M.S.S. Brooks, R. Ahuja, J. Alloys Compd. 296 (2000) 27.
[22] F. Birch, Phys. Rev. 71 (1947) 809.
[23] F.D. Murnaghan, Am. J. Math. 49 (1937) 235.
[24] B.R. Lawn, V.R. Howes, J. Mater. Sci. 16 (1981) 2745.
[25] Materialprüfungsamt Nordrhein-Westfalen, Dortmund, Germany, Cert. No. 43000813–43001215, 2000.
[26] J. Spino, J. Cobos, F. Rousseau, J. Nucl. Mater. 322 (2003) 204.
[27] P.G. Lucuta, Hj. Matzke, R.A. Verall, B.J. Palmer, J. Nucl. Mater. 178 (1991) 48.
[28] J. Cobos, D. Papaioannou, J. Spino, M. Coquerelle, J. Alloy Compd. 271–273 (1998) 610.
[29] M.P. Pechini, US Patent No. 3.330.697, 11 July 1967.
[30] M.C. Pujol, J. Spino, J. Eur. Ceram. Soc., to be published.
[31] S. Heathman, personal communication, unpublished result, 2002.
[32] W.B. Holzapfel, in: R. Pucci, G. Piccitto (Eds.), Molecular Solids Under Pressure, North-Holland, Amsterdam, 1990, p. 61.
[33] P. Vinet, J. Ferrante, J.R. Smith, J.H. Rose, J. Phys. C 19 (1986) L467.
[34] M. Kumar, Physica B 217 (1996) 143.
[35] T.R.G. Kutty, A.K. Sengupta, C. Ganguly, Eur. Appl. Res. Rept. – Nucl. Sci. Tech. 7 (1990) 1473.
[36] E. Grüneisen, Ann. Phys. 12 (1912) 257.
[37] L. Vocadlo, J.P. Poirer, G.P. Price, Am. Mineral. 85 (2000) 390.
[38] A.G. McLellan, The Classical Thermodynamics of Deformable Materials, Cambridge University, Cambridge, 1980.
[39] M.A. Blanco, A.M. Pendás, E. Francisco, J.M. Recio, R. Franco, J. Mol. Struct. (Theochem.) 368 (1996) 245.
[40] K.H. Kang, H.J. Ryu, K.C. Song, M.S. Yang, J. Nucl. Mater. 301 (2002) 242.
[41] M.C. Pujol, J. Spino, to be published.
[42] J.K. Fink, J. Nucl. Mater. 279 (2000) 1.
[43] Hj. Matzke, P.G. Lucuta, R.A. Verall, J. Henderson, J. Nucl. Mater. 247 (1997) 121.
[44] R.M. Hazen, L.W. Finger, J. Geophys. Res. 84 (1979) 6723.
[45] J. Smyth, S.D. Jacobsen, R. Hazen, Rev. Mineral. 41 (2000) 157.
[46] T. Petit, B. Morel, C. Lemaignan, Philos. Mag. B 73 (1996) 893.
[47] S.L. Dudarev, G.A. Botton, S.Y. Savrasov, Z. Szotek, W.M. Temmerman, A.P. Sutton, Phys. Status Solidi (a) 166 (1998) 429.
[48] R.W. Grimes, C.R.A. Catlow, Philos. Trans. Roy. Soc. London A 335 (1991) 609.
[49] K. Yamanada, K. Kurosaki, M. Uno, S. Yamanaka, J. Alloy Compd. 307 (2000) 1.